Advances in Science and Technology Research Journal

Advances in Science and Technology Research Journal, 2027, 21(1), 14–28
https://doi.org/10.12913/22998624/226680
ISSN 2299-8624, License CC-BY 4.0

Received: 2026.06.23
Accepted: 2026.11.15
Published: 2026.12.01

Multi-criteria optimization of unmanned aerial vehicles medical transport corridors in urban environments based on cost surface analysis

Jarosław Tatarczak[1*], Justyna Baran-Tatarczak[2]

[1] Faculty of Mathematics and Information Technology, Lublin University of Technology, 20-618 Lublin, Poland
[2] JBT Solid Plan, Poland
* Corresponding author's e-mail: j.tatarczak@pollub.pl

ABSTRACT

The dynamic development of medical logistics utilizing unmanned aerial vehicles (UAVs) in time-critical missions requires a careful balance between operational efficiency and stringent ground risk class (GRC) safety requirements within dense urban environments. This study introduces and implements a multi-criteria optimization model for autonomous beyond visual line of sight (BVLOS) medical flight corridors based on spatial cost surface analysis. The proposed methodology integrates urban planning structures with the SORA risk assessment framework. Utilizing a dasymetric mapping technique, a spatial disaggregation of demographic data was performed, shifting from homogeneous administrative districts to a continuous population presence probability model based on urban capacity indicators derived from the draft General Plan of the City of Lublin. Using the analytic hierarchy process (AHP), specific weights were assigned to five operational criteria, with human exposure defined as the overriding component of the model. The final spatial resistance map was generated through multi-criteria evaluation (MCE), and the optimal trajectories were calculated using the least-cost path (LCP) algorithm. To evaluate model robustness and address shifts in operational priorities, a scenario-based sensitivity analysis was conducted via weight permutation. Validation of the model across selected healthcare facilities in Lublin demonstrated that LCP corridors reduce the operational population exposure risk (*Rop*) by an average of 74.38% compared to geometric shortest paths. Despite the extended trajectories, these routes guarantee a 22–40% time advantage over ground emergency medical services (EMS). Furthermore, network analysis revealed that spatial optimization does not significantly affect cellular handover dynamics, maintaining a comparable frequency of network switches across both routing strategies. The developed method serves as a robust decision support tool, enabling the safe operationalization of urban air mobility (UAM) networks integrated with municipal spatial planning.

Keywords: UAV, medical logistics, cost surface, GIS analysis, path planning, urban zone.

INTRODUCTION

The dynamic development of urban air mobility (UAM) concepts opens up entirely new perspectives for contemporary urban logistics [1]. Unmanned medical transport represents a primary application area for these systems due to its inherently time-critical nature [2]. In particular, emergency operations like blood component distribution cannot afford delays caused by urban ground congestion [3]. Because these high-priority medical payloads are characterized by low physical mass, they perfectly match current multirotor constraints while achieving excellent public acceptance [4, 5]. Furthermore, the predictable point-to-point network structure of healthcare networks minimizes operational uncertainty [6], rendering medical logistics the most legally justified direction for autonomous beyond visual line of sight (BVLOS) flights [7].

Spatial and organizational challenges

However, urban space is a highly heterogeneous environment, saturated with legal-spatial constraints and physical barriers [1], as well as social challenges [4]. The integration of autonomous systems into the urban fabric extends beyond purely technological frameworks, presenting a complex organizational and planning challenge [8]. Furthermore, designing secure aerial corridors requires the implementation of advanced geospatial decision support tools (DST) [8], as well as mathematical optimization models to properly position network assets like warehouses and drone hubs [6].

However, urban space is a highly heterogeneous environment, saturated with legal-spatial constraints and physical barriers [1], as well as social challenges [4]. Moreover, complex terrain conditions and environmental obstacles introduce distinct operational limitations that heavily restrict safe UAV navigation and reconnaissance capabilities [9]. The integration of autonomous systems into the urban fabric extends beyond purely technological frameworks, presenting a complex organizational and planning challenge [8]. Furthermore, designing secure aerial corridors requires the implementation of advanced geospatial decision support tools (DST) [8], alongside comprehensive path-planning methodologies and optimization frameworks [10], as well as mathematical optimization models to properly position network assets like warehouses and drone hubs [6].

The municipal general plan

A significant, yet novel component of the aforementioned process is the direct implementation of the functional structure of planning zones defined within the framework of new General Municipal Plan [11]. Formal land use constitutes a justified proxy variable, enabling precise quantification of ground risk [12] as well as the potential structure and density of population distribution [13] across different urban areas. Consequently, planning data becomes the foundation for route optimization, allowing for the minimization of public risk already at the strategic planning stage [14] and providing an objective basis for parameterizing the ground risk class (GRC) within the unified Specific Operations Risk Assessment (SORA) methodology [15].

Selecting the optimal cruising altitude

In the multi-criteria flight trajectory design process for medical UAVs, a key factor determining operational efficiency is the proper selection of the cruising altitude [14], which must reconcile strict regulatory constraints [15] with the physical characteristics of the atmospheric boundary layer. Due to the specific nature of medical transport, these operations should be conducted BVLOS, automatically qualifying them for the "Specific" category [15]. Within this legal framework, an altitude of 100–120 meters above ground level (AGL) represents the optimal operational range (max. 120 m AGL for the open category), allowing for the maintenance of standard, simplified risk mitigation procedures within the SORA methodology [15]. Exceeding the 120-meter AGL threshold implies entering airspace with an increased collision risk, which drastically complicates the risk assessment process, requires advanced detect and avoid systems, specialized personnel training, and individual approvals from the Polish Civil Aviation Authority, thereby significantly limiting the scalability of the transport system.

Urban microclimate

Lowering the UAV flight altitude below the dominant rooftop level proves to be highly inefficient and hazardous in an urban environment [17]. This lower airspace is characterized by unstable wind fields and mechanical disturbances induced by complex building geometries [17, 18]. For multirotor platforms, operating within this turbulent urban roughness sublayer disrupts flight stability and forces continuous control adjustments [18]. This mode of operation severely disrupts the optimal energy consumption profile of the entire logistics platform. Consequently, to maintain operational range and stability, flight trajectories must be optimized above this obstacle layer [19].

Operational safety and population protection

To systematically execute this optimization, the proposed model evaluates the target altitude layer (120 meters AGL) through a unified cost surface comprising three complementary spatial cost dimensions. The first crucial component is ensuring operational safety and protecting sensitive structures [15]. At the assumed cruising

altitude, unmanned platforms generally operate above standard urban infrastructure. Exceptions, however, include urban architectural landmarks and tall high-volume buildings (office buildings, industrial facilities, masts), which require three-dimensional identification and avoidance, while simultaneously incorporating safety buffers over high-density population zones determined on the basis of municipal planning documentation [11].

Command and control network

An equally important cost dimension is the resilience of the Command and Control (C2) network. At cruising altitudes above 100 meters, the absence of terrain obstacles ensures direct line-of-sight with multiple transmitters simultaneously. Paradoxically, this can degrade signal quality by triggering inter-cell broadband interference and forcing continuous, economically unjustified link switching between cells – known as the handover ping-pong effect [20, 21]. The model must therefore incorporate communication infrastructure constraints to evaluate link stability along the designated corridors.

Practical implementations in urban medical logistics

The operational feasibility of such multi-criteria trajectories is reflected in real-world applications, where point-to-point aerial connections constitute a permanent component of healthcare networks [16]. Practical implementations include the regular transport of laboratory samples between hospitals, which allows for bypassing ground congestion and reducing transport time from several dozen to just a few minutes [16]. However, designing these corridors requires minimizing sudden vertical maneuvers, as flight-induced vibrations can threaten the structural integrity of sensitive biological materials [22]. Recent studies demonstrate that with appropriate damping and trajectory stabilization, UAV operations preserve sample quality, offering a viable and safe alternative to traditional hospital pneumatic systems [23].

Spatial cost surface analysis

To eliminate the identified hazards, this study implements a multi-criteria transport corridor design strategy based on spatial cost surface analysis. This approach allows for the optimal integration of formal-legal, environmental, and topographical constraints into a single, coherent model. By translating land-use designations (functional zones of Municipal General Plan) and variations in surface morphology into a mathematical cost space, the routing algorithm automatically bypasses areas with elevated ground risk and optimizes the trajectory relative to the urban surface topography. As a result, the determined trajectory minimizes the global cost of the aerial operation, ensuring safe and regulatory-compliant separation from the urban fabric at the assumed altitude, while simultaneously maintaining logistical efficiency.

Research gap and objective

While various path-planning algorithms exist, there remains a noticeable scarcity of methodologies that directly and systematically integrate recently updated national spatial planning frameworks – specifically municipal functional zones – with high-resolution analyses of topographical conditions at targeted UAM operational altitudes. This study aims to address this limitation by developing a comprehensive geoinformation framework for designing medical UAV transport corridors using multi-criteria cost space modeling. A key advantage of the proposed methodology is its high reproducibility; since the structural requirements of the new Municipal General Plan are nationally standardized, the workflow can be easily adapted and replicated across other urban areas in Poland. The practical implementation and operational verification of the model are presented through a case study of Lublin (Poland) – a city characterized by diverse terrain morphology – by conducting simulations of autonomous delivery flights between key hospital complexes in a heterogeneous urbanized environment.

Research hypothesis

The following research hypothesis was formulated in this study – integrating multi-criteria surface cost modeling based on municipal planning documentation and infrastructural data allows for the determination of UAV transport corridors in an urban environment that significantly minimize operational risk to the ground population, while simultaneously maintaining a time-efficiency advantage over privileged ground transport.

Methodology and data sources

In order to precisely quantify the GRC within the SORA methodology, a key phase of the analysis involved shifting away from averaged data aggregated at the administrative unit level towards continuous population density surface modeling. The research procedure consisted of the following stages:

1. Source data acquisition and characterization.
2. Dasymetric mapping and data disaggregation.
3. Generation of the population presence probability map.

Information regarding the population broken down by individual districts of the city of Lublin was obtained from the official reporting resources of the Lublin City Hall (May 2026).

The structure of boundaries and land-use designations of the functional zones was acquired from the spatial database of the Lublin City Hall. Due to the current legislative status, the digital compilation of the draft General Plan of the Municipality was utilized in the analyses (pre-final version, currently undergoing the formal review and opinion-molding procedure, May 2026).

Traditional population assignment to entire districts distorts the risk profile by indicating population presence in uninhabited areas (e.g., parks, water bodies). Therefore, a multi-criteria spatial disaggregation method (dasymetric mapping) was applied. The weight (population redistribution coefficient) for each planning zone was determined based on the relationship between two geometric and urban parameters specified in the draft general plan:

- Functional zone area (A) – which determines the physical spatial capacity,
- Building intensity index (I, equivalent to Floor area ratio – FAR) – defined in urban planning as the ratio of a building's total floor area to the size of the piece of land upon which it is built. It serves as a direct indicator of potential housing capacity and the degree of concentration of building structures.

The mathematical algorithm proportionally disaggregated the global population numbers previously assigned to a given district, allocating them within the boundaries of individual planning zones based on the building intensity index specified in the draft general plan, which directly defines their spatial urban capacity. The population after allocation to the planning zones was calculated as follows:

$$P_s = P_d \cdot \frac{A_s \cdot I_s}{\sum_{i \in d}(A_i \cdot I_i)} \quad (1)$$

where: P_s – estimated population in a given planning zone s, P_d – number of residents in a given district d, A_s – area of the analyzed planning zone s, I – building intensity index for a given planning zone s

The final output of the procedure is a surface cost raster (population density surface model), representing a detailed, intra-district population density distribution. This data structure enables the identification of zones with an increased probability of population exposure to accident risks, down to the level of a specific planning micro-corridor, thereby redefining previous, homogeneous zonal approaches. The result is presented using the example of a selected district of Lublin in Figure 1, which illustrates the transition from a homogeneous demographic database to a continuous surface model of population presence probability.

Multi-criteria surface cost modeling using the AHP procedure

Efficient determination of optimal flight routes for medical UAVs in a dynamic urban environment requires a multi-criteria categorization of geographic space. A key engineering challenge at this stage is the transformation of qualitative and descriptive urban functions, as well as spatial operational barriers, into normalized measurable values that can be processed by routing algorithms.

The foundation for the entire decision-making model is a unified risk parameterization matrix, which defines a rigid scoring framework for five key operational criteria on a five-point discrete scale (Table 1). The adopted evaluation scale (where: 1 – very low risk; 5 – critical risk) allows for the standardization of demographic, technical, spatial, and social variables. Through this standardization, heterogeneous information layers are brought to a common mathematical denominator, enabling their further synthesis using weights determined via Saaty's Analytic Hierarchy Process (AHP).

In the context of unmanned aircraft operations in urban environments (e.g., the city of Lublin), the individual factors described in Table 1 are characterized by varying degrees of criticality regarding the overall safety level of a logistics mission. The

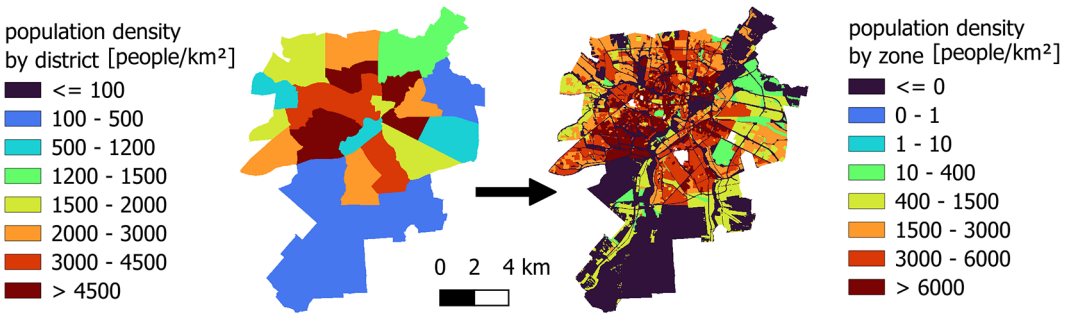


Figure 1. Dasymetric disaggregation of population density: transition from a homogeneous district-level model (left) to a high-resolution zone-specific population model (right) for Lublin city

process of scale unification (1–5) alone does not reflect the hierarchy of importance of these criteria. To determine objective and mathematically consistent weights for each cost layer, the AHP method was implemented. Taking into account the primacy of protecting human life on the ground and the ground risk class mitigation guidelines within the SORA methodology [15], criterion K_1: Human Exposure was defined as the overriding component of the model. The expert pairwise comparison matrix takes the following structural form:

$$M = \begin{pmatrix} & K1 & K2 & K3 & K4 & K5 \\ K1 & 1 & 3 & 5 & 7 & 9 \\ K2 & 1/3 & 1 & 3 & 5 & 7 \\ K3 & 1/5 & 1/3 & 1 & 3 & 5 \\ K4 & 1/7 & 1/5 & 1/3 & 1 & 3 \\ K5 & 1/9 & 1/5 & 1/5 & 1/3 & 1 \end{pmatrix} \quad (2)$$

As a result of executing the mathematical AHP procedure (determining the eigenvector of matrix *M*), the following decision weights were obtained for the individual input layers:

To evaluate the robustness of the developed model and address potential shifts in municipal or stakeholder priorities, a scenario-based sensitivity analysis was conducted via weight permutation (Table 2). Instead of local mathematical perturbations, three distinct operational philosophies were tested - focusing on human safety (Variant 1), UAV operational safety and recovery (Variant 2), and social acceptance and privacy (Variant 3) – to observe their spatial impact on the resulting least-cost path (LCP) trajectories.

To verify the logical consistency of the expert judgments, the consistency ratio (CR) was calculated: the maximum eigenvalue of the matrix λ_{max}=5.37, the consistency index C_I=0.09, and

Table 1. Spatial risk categorization matrix for UAV missions on a 1–5 scale

Criterion	1 (very low)	2 (low)	3 (Moderate)	4 (High)	5 (Very high/critical)
K_1: Human exposure	<0.1 person./km²	0.1–500 person./km²	500–1500 person./km²	1500–3000 person./km²	>3000 person./km²
K_2: Emergency landing	Numerous flat, open areas (fields, squares)	Limited but safe locations (wide residential roads, green squares	Urbanized spaces with restricted access (parking lots, gardens)	Dense infrastructure (dense urban tree cover, single-family housing)	No available spots (dense, high-rise volumetric development)
K_3: Surrounding statics	Static terrain (no permanent pedestrian or vehicular traffic routes)	Local traffic with very low intensity (e.g., homestead development)	Moderate traffic (collector streets, pedestrian-vehicular zones)	Heavy traffic (shopping centers, transit hubs)	Main arterial roads and transit routes (continuous vehicular traffic)
K_4: UAV and payload recovery	Public terrain, completely open to ground crews	Public terrain with minor obstacles (e.g., curbs, ditches, curves/ bends)	Fenced or private terrain (single-family buildings)	Difficult to access terrain (dense thickets, wetlands)	Restricted/closed area, inaccessible (high-rise roofs, large industrial complexes)
K_5: Privacy	No possibility of observing people or private properties	Publicly accessible green squares and city parks	Public utility facilities of a mass character	Preschools, schools, private recreational gardens	Residential buildings

the consistency ratio for n=5 (RI=1.12) yielded CR=8.42%. Since the obtained CR value is below the widely accepted 10% threshold in the AHP method (CR<0.1), the pairwise comparison matrix satisfies the consistency requirement.

Determining the weight vector using the AHP method and defining the risk rating scale (1–5) enabled the transition from theoretical assumptions to the mathematical and spatial modeling phase within the GIS environment. The primary objective of this stage was the operationalization of the planning zones – specifically, translating the 13 formal land-use classes derived from the draft general plan into measurable resistance (cost) values for UAV flights.

This process was implemented by evaluating each planning zone against the five defined criteria (K_1-K_5). A methodologically crucial aspect was determining the values for the primary criterion, K_1 (Human Exposure). To eliminate the subjectivity of expert assessment, the parameterization of this factor was based directly on the results of the preceding dasymetric modeling. For the remaining technical and social criteria (K_2-K_5), sub-scores were assigned based on expert judgment, drawing on the analysis of the morphological and urban characteristics of individual land-use designations. Consequently, a unified evaluation matrix was developed (Table 3), where each zone received a complete set of sub-scores on a scale of 1–5. The final spatial cost for each zone was calculated using a weighted average, which forms the cornerstone of Multi-Criteria Evaluation (MCE) methods:

$$S_{cost} = \sum_{i=1}^{n} (K_i \cdot w_i) \tag{3}$$

where: K_i – denotes the score of the zone for a given criterion, w_i – normalized weight of this criterion determined via the AHP procedure.

To thoroughly examine the sensitivity of the model to the modification of criterion weights, a two-way analysis of variance without replication was conducted, treating planning zones as blocks and the variants (V_1, V_2, V_3) as experimental conditions. The test results revealed statistically significant differences among the analyzed variants ($F(2, 24)=6.43$, $p=0.0058$). This indicates that the model exhibits high sensitivity to changes in operational priorities - correctly reacting to modifications in the weight structure - while simultaneously maintaining a strong mutual correlation between cost structures, which confirms its spatial stability and robustness.

In order to perform an objective, multi-criteria assessment and comparison of alternative flight route variants for medical (UAVs), a system of evaluation metrics was introduced. The defined indicators (Table 4) combine geometric, logistical, infrastructural characteristics with spatial and social risk parameters, allowing for full operationalization and evaluation of the generated transport routes.

Time efficiency

In order to determine the reference arrival time (T_{amb}) of a ground emergency medical service (EMS) team, a methodology based on routing algorithms available within the Google Maps application programming interface (API) was applied. The baseline travel time data were retrieved during a period of minimal traffic volume (off-peak hours) to simulate optimal, best-case conditions for ambulance transport This approach allows for the inclusion of the actual geometry of the road network, legal and organizational conditions (including traffic organization, one-way streets, and maneuver restrictions), as well as dynamic parameters of urban traffic flows, which would be impossible to model precisely using a static vector model.

Table 2. Normalized priority weights for individual operational criteria determined using the AHP method

Criterion symbol	Criterion name	Calculated weight (*w*)		
		Variant 1 human safety	Variant 2 UAV safety	Variant 3 privacy
K_1	Human exposure	50.28%	6.78%	26.02%
K_2	Emergency UAV landing	26.02%	50.28%	13.44%
K_3	Surrounding statics	13.44%	26.02%	6.78%
K_4	UAV and payload recovery	6.78%	13.44%	3.48%
K_5	Privacy	3.48%	3.48%	50.28%

Table 3. Multi-criteria evaluation matrix of planning zones – category weights, sub-scores, and the resulting baseline cost for flight trajectory determination

Zone symbol	Category / name of planning zone	K_1	K_2	K_3	K_4	K_5	$S_{cost}(V_1)$	$S_{cost}(V_2)$	$S_{cost}(V_3)$	A_s/A_c %
SR	Agricultural production	1	2	1	1	1	1.26	1.50	1.13	0
SO	Open	1	3	3	3	2	1.96	2.83	1.98	23.16
SC	Cemetery	3	3	1	1	2	2.56	2.18	2.29	1.72
SN	Green and recreation	3	3	2	3	2	2.83	2.70	2.43	14.49
SZ	Farmstead development	3	3	3	2	4	2.97	2.90	3.47	0.26
SI	Infrastructure	3	4	3	1	1	3.06	3.16	2.06	2.79
SP	Industrial	4	3	2	2	1	3.23	2.60	2.15	7.81
SG	Extractive industry	4	3	4	3	1	3.57	3.26	2.32	0.003
SK	Transport	4	4	1	5	3	3.63	3.32	3.33	7.85
SJ	Single-family residential	4	4	4	3	4	3.93	3.87	3.97	19.89
SU	Service	5	4	3	4	2	4.30	3.74	3.19	7.73
SW	Multi-family residential	5	5	2	3	4	4.43	3.92	4.22	13.08
SH	Large-scale retail	5	4	4	5	2	4.50	4.13	3.29	1.24

Note: *A_s/A_c - the ratio of the total area of all zones of a given type to the total area of the city of Lublin.

The baseline travel time value was calibrated using a correction factor (k) that accounts for the vehicle's priority status in road traffic. Based on the analysis conducted in the literature [24], the factor value was set at 0.7675 (corresponding to 76.75% of a standard vehicle's travel time), determined as the arithmetic mean for various urban congestion conditions.

Building exposure

Another indicator quantifies the risk to urban buildings associated with UAV operations. A buffer with a radius of 74 m from the mission route axis was determined. The buffer size reflects a worst-case scenario defined as a complete loss of power and propulsion at the least favorable

Table 4. Evaluation metrics structure for medical UAV flight paths

Metric name	Symbol	Unit	Description	Remarks
Total UAV route length	L_{UAV}	m	Total length of the generated UAV flight path vector	-
UAV flight time	T_{UAV}	s	Cargo delivery time at the assumed cruise speed	v_{UAV} = 15 m/s $T_{landing}$ = 30s $T_{UAV} = 2 \bullet T_{landing} + T_{flight}$
Time efficiency (EMS vs. UAV)	δ	%	Percentage and absolute time savings of the UAV flight relative to the emergency ambulance travel time	k = 0.7675
Number of buildings in the buffer	B	count	Total number of buildings within the flight buffer zone	v_{UAV} = 15 m/s H_{UAV} = 120 m AGL buffer = 74 m
Mean building area in buffer	B_m	m^2	Mean area of buildings within the flight buffer zone	v_{UAV} = 15 m/s H_{UAV} = 120 m AGL buffer = 74 m
Total route surface cost	S_{cost}	[-]	Represents the total cost of movement along the route within the surface cost	Refer to Table 3
Total operational risk to population	R_{op}	person / s	Cumulative, relative indicator of operational risk along the entire flight trajectory of the UAV	-
Nearest neighbor index BTS	nn_{index}	%	Distribution pattern of Base Transceiver Stations for a given flight rout	For a 1000 m buffer
Number of BTS in a buffer	n_{BTS}	count	Number of Base Transceiver Stations in buffer along the UAV flight route	For a 1000 m buffer
Number of handovers between BTS	h_{UAV}	count	Represents the number of UAV route intersections based on Voronoi tessellation	For a 1000 m buffer

operational point: at the maximum flight altitude (h_{max} = 120 m) and the nominal cruise speed (v_{UAV} = 15 m/s). Adopting a rigorous computational approach that neglects aerodynamic drag forces, the ballistic trajectory of the UAV's uncontrolled descent was described by the classic equation of a horizontal projectile motion.

Operational risk to ground population

In order to determine the total operational risk along the entire flight trajectory (R_{op}), the route was discretized into n population density raster cells (i). The baseline ground risk model [25] was extended to include the kinematic parameters of the UAV, replacing the exposure time with the ratio of the route length within a given raster cell (L_i) to the constant cruise speed of the craft (v_{UAV}):

$$R_{op} = A_{crash} \cdot \sum_{i=1}^{n} \left(D_i \cdot \frac{L_i}{v_{UAV}} \right) \quad (4)$$

where: A_{crash} – total UAV impact area at the moment of loss of control [m²], D_i – dasymetric population density in the i-th raster cell [person/m²], L_i – length of the route section within the i-th raster cell [m], v_{UAV} – assumed constant cruise speed of the UAV [m/s].

Such a formulation allows for the direct integration of risk modeling [25] with spatial routing algorithms within a GIS environment, where the cost of traversing a raster cell (which serves as an element of a dasymetric density map) is strictly linked to the route geometry [25]. The parameter A_{crash} defines the total projected area of the impact zone on the ground plane at the moment of losing control over the drone. It represents the relationship between the dimensions of the UAV and a human in relation to the adopted glide angle of the aircraft, expressed by the formula [25]:

$$A_{crash} = \pi(r_{UAV} + r_h)^2 + \frac{2(r_{UAV} + r_h)H_h}{\tan(\theta)} \quad (5)$$

where: r_{UAV} – UAV radius (m), r_h – human radius (m), H_h – human height (m), θ – angle of inclination at the moment of impact.

For the purpose of the analysis, the following parameters were adopted: the UAV radius (r_{UAV}) as 0.5 meters, the human radius (r_h) as 0.3 meters, the human height (H_h) as 1.8 meters, and the drone glide angle (θ) of 45°. Following the calculations, the theoretical crash area *Acrash* was determined to be 4.89 m², which was subsequently rounded to 5 m² to incorporate a conservative safety margin.

Base transceiver stations

The stability assessment of the C2 link was conducted based on a spatial analysis of the locations of Base Transceiver Stations (BTS) operating in the LTE800 band. The investigation of the surroundings of the designated routes included counting the total number of masts within distance bands up to 1000 m and a statistical network analysis using the average nearest neighbor (ANN) index. Additionally, the geometry of Voronoi polygons was used to simulate dynamic network handovers. This tessellation allowed for the mathematical determination of theoretical coverage areas, where a given transmitter constitutes the closest and optimal access point for the UAV receiver.

Medical facilities location

The model incorporates three key medical facilities within Lublin, representing diverse morphological, demographic, and spatial conditions of the city. A detailed list of the nodal points, along with their geographic locations and spatial characteristics, is provided in Table 5.

Table 5. List of medical facilities used in the analysis

Symbol	Medical facility name	Geographic coordinates	Location characteristics in the model
A	Stefan Cardinal Wyszynski Regional Specialist Hospital	51.23954° N 22.50353° E	Western part of the city. The surroundings consist mainly of green belts and low-rise residential buildings.
B	University Clinical Hospital No. 4 in Lublin	51.25874° N 22.56453° E	Downtown area. Very high population density and dense structural development; a zone with high take-off and landing risk.
C	John of God Public Regional Hospital	51.21545° N 22.56977° E	Southern part of the city. A node connecting industrial-warehouse districts and medium-density residential areas.

The flight routes were established on an 'all-to-all' basis as a combination without repetition, allowing for the determination of 3 unique trajectories connecting the analyzed medical facilities. Two route variants between each point were adopted in the analysis: the shortest path (SP) and the least-cost path (LCP). The routes were generated using the QGIS software supported by GRASS GIS modules, which execute a wavefront expansion graph-search over a cumulative cost surface mapped at a 10x10 meter grid resolution. This discrete grid-based global approach mathematically guarantees global optimality within the defined state-space, preventing the routing algorithm from becoming trapped in local minima. Restricted airspaces, which are typically excluded from UAV flights – such as military areas, penitentiary institutions, or uniform services facilities – were excluded from the analysis.

RESULTS AND DISCUSSION

This chapter presents the results of modeling flight trajectories for UAVs performing medical transport missions between selected hospitals (nodes A, B, and C) within the area of Lublin. The primary focus of the evaluation is to compare the flight corridors determined by the LCP algorithm – which is based on a multi-criteria assessment of ground risk and infrastructural conditions – with the reference Shortest Paths in straight lines.

Initially, a sensitivity analysis was conducted for route A–B, with its spatial visualization presented in Figure 2 and the corresponding numerical results in Table 6. Only subsequently were the remaining routes analyzed using Variant 1.

The results for route A-B presented in Table 6 demonstrate that the LCP algorithm effectively reduces both total and unit surface costs (S_{cost}) compared to the SP across all priority variants. Although in Variant 1 (human safety) and Variant 3 (privacy) LCP routes are slightly longer (L_{UAV}) and require a longer flight time (T_{UAV}), under Variant 2 (UAV safety) the LCP algorithm allows for a shorter and faster path than SP. Furthermore, despite a higher number of buildings (B) within the buffer zone for LCP, their mean area (B_m) is significantly smaller, confirming that large-scale structures are bypassed in favor of smaller, scattered developments. A key result is the drastic reduction of operational risk to the ground population (R_{op}) achieved by LCP, which drops to 16.98% in Variant 3 and 25.78% in Variant 1 of the value determined for the traditional SP route.

Following the sensitivity analysis, the evaluation of the obtained results continues with a visual analysis of the geometric configuration of the generated air corridors in relation to the city's spatial. A comprehensive overview of all LCP and SP trajectory routes is presented in Figure 3.

Visualizing the generated baseline cost surface $S_{cost}(V_1)$ in direct comparison with the determined flight trajectories allows for a spatial evaluation of the LCP algorithm's efficiency. The cost raster, which synthesizes the multi-criteria evaluation of planning zones and population density, clearly reflects the varying resistance of the urban space. Dark tones represent safe zones (e.g., open and green areas) and light areas concentrate the highest operational risk (e.g., commercial and residential zones). The analysis of the path lines proves that LCP trajectories flexibly adapt their geometry to environmental conditions, bypassing key cost accumulations, whereas the reference SP

Table 6. Comparative analysis of routing strategies and metrics for Route A-B across distinct operational priority Variants (1–3)

Symbol	Route A-B	Variant 1 human safety			Variant 2 UAV safety			Variant 3 privacy		
	Unit	LCP	SP	LCP/SP	LCP	SP	LCP/SP	LCP	SP	LCP/SP
S_{cost}	[-]	17 399	19 328	90.02%	16 315	17 251	94.57%	14 182	16 749	84.67%
	1 / m	3.27	4.07	80.30%	3.63	3.64	100.27%	2.57	3.52	73.01%
L_{UAV}	m	5 328	4 753	112.10%	4483	4 753	94,32%	5512	4 753	115.97%
T_{UAV}	min	6.92	6.28	110.18%	5.98	6.28	95.22%	7.12	6.28	113.43%
B	count	232	70	331.43%	196	70	280.00%	375	70	535.71%
B_m	m^2	576.97	859.01	67.17%	459.24	859.01	53,46%	310.76	859.01	36.18%
R_{op}	pers./s	2.50	9.72	25.78%	5.41	9.72	55.66%	1.65	9.72	16.98%

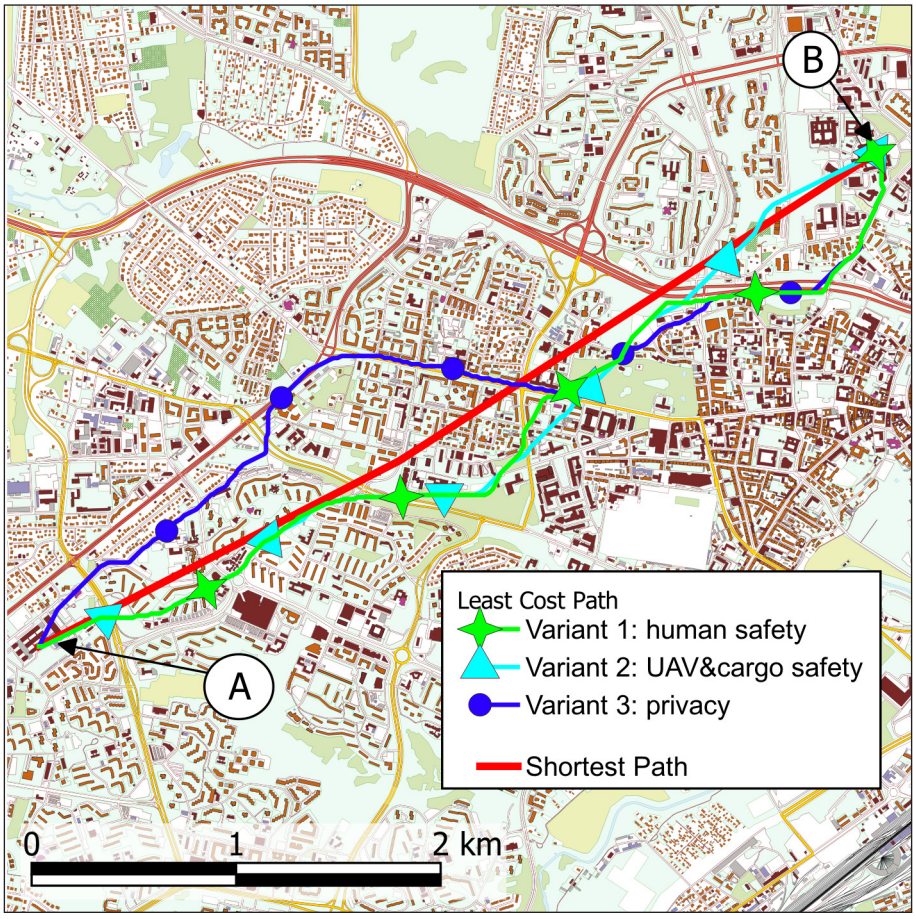


Figure 2. UAV flight trajectories on the A–B route for three scenarios (Variants 1–3) against the background of Lublin's planning zones. Legend: A, B – locations of medical facilities. Base map data sourced from the topographical objects database (BDOT10K) [26]

rigidly cut through regions of maximum resistance in a straight line. The baseline cost surface distribution is illustrated in Figure 4.

Another key element of the results analysis is the quantitative assessment of the basic geometric and cost parameters of the designated air corridors. To verify the efficiency of the Least-Cost Path algorithm, the key operational indicators for the optimized routes (LCP) were compared with the reference Shortest Paths across three studied inter-nodal relations (A-B, A-C, B-C). A summary of this mathematical and spatial data is presented in Table 7.

An analysis of the relative parameters confirms the high efficiency of the LCP algorithm in minimizing operational risk. At the cost of a relatively small increase in route length compared to the SP variant – by 12.1% (A-B), 3.24% (A-C), and 9.91% (B-C), respectively – a reduction in the total spatial cost S_{cost} was achieved, with a maximum decrease of over 27% for the B-C relation. Crucially, the unit cost S_{cost}/m for the LCP corridors remains at a similarly low level across all relations (within the range of 3.10–3.27), whereas for the SP routes, the unit cost is higher by an average of 26.3% compared to the LCP.

In the A-B route, a higher number of buildings (B) was recorded within the 74 m buffer from the route centerline for the LCP route than for the SP. This is due to the fact that the AHP model did not include the direct number of buildings as a separate criterion, but was instead based on land-use classes. Concurrently, it was observed that despite the quantitative increase in the number of buildings within the buffer, their mean area was significantly reduced (to 576.97 m^2). This indicates that the A-B route in the LCP variant effectively bypassed large-scale buildings compared to the reference SP route, directing the flight corridor over areas with smaller, scattered development characterized by a lower risk priority.

In all analyzed UAV routes (A-B, A-C, B-C), the LCP trajectories are characterized by distinctly lower R_{op} values than the reference SP lines.

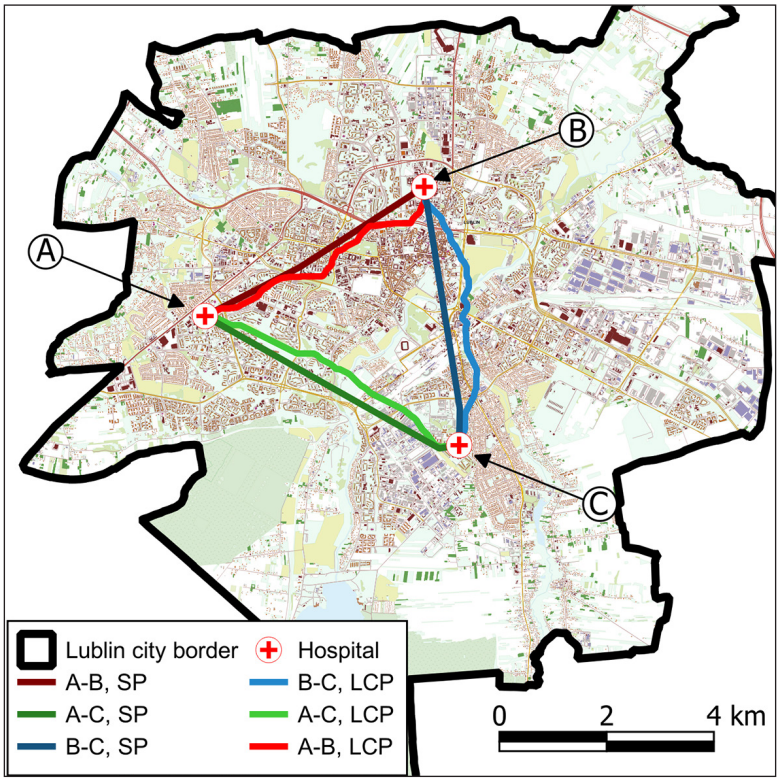


Figure 3. Spatial visualization of UAV flight trajectories (LCP vs. SP; Variant 1: human safety) against the background of Lublin's planning zones. Legends: LCP – Least Cost Path; SP – Shortest Path; A, B, C – locations of medical facilities. Data from the topographical objects database (BDOT10K) [26] was used as the base map

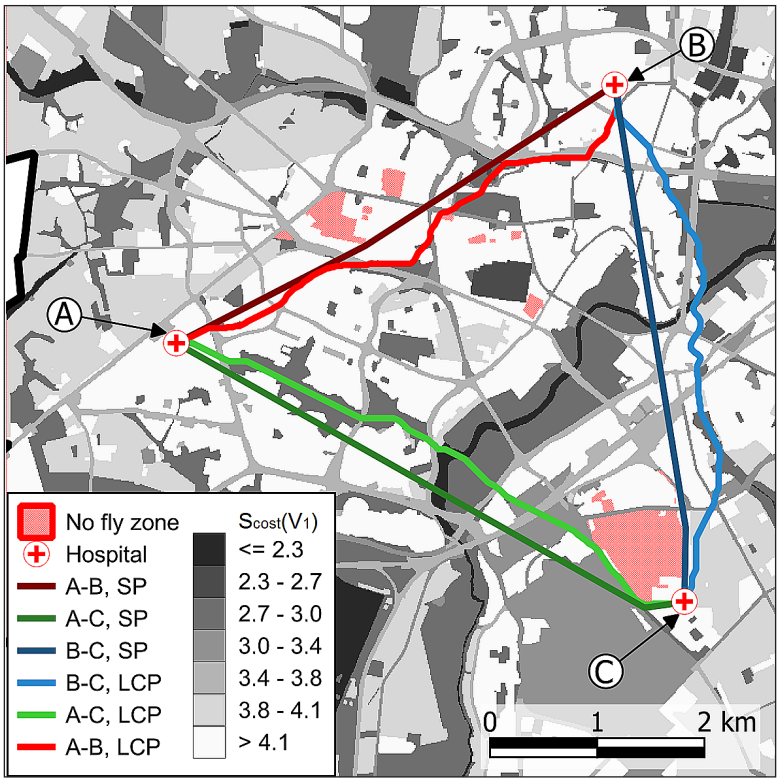


Figure 4. Spatial distribution of the baseline cost surface $S_{cost}(V_1)$ overlaid with UAV flight trajectories (LCP vs. SP) in the area of Lublin. Legend: LCP – least cost path; SP – shortest path; A, B, C – locations of medical facilities

Table 7. Comparative analysis of UAV routing strategies (LCP vs. SP) based on surface cost, route length and flight time, building exposure, and operational risk for Variant 1

Symbol	Routes	A-B			A-C			B-C		
	Unit	LCP	SP	LCP/SP	LCP	SP	LCP/SP	LCP	SP	LCP/SP
S_{cost}	[-]	17 399	19 328	90.02%	17 455	20 401	85.56%	16 626	20 401	81.49%
	1 / m	3.27	4.07	80.30%	3.14	3.78	82.88%	3.10	4.19	74.15%
L_{UAV}	m	5 328	4 753	112.10%	5 566	5 392	103.24%	5 355	4 872	109.91%
T_{UAV}	min	6.92	6.28	110.18%	7.18	6.99	102.78%	6.95	6.41	108.36%
B	count	232	70	331.43%	199	222	89.64%	564	685	82.34%
B_m	m^2	576.97	859.01	67.17%	713.47	778.37	91.66%	243.58	296.42	82.17%
R_{op}	pers./s	2.50	9.72	25.78%	2.07	10.36	19.96%	2.36	7.59	31.13%

This result confirms that the weights introduced into the model (according to the AHP method) and the multi-criteria evaluation analysis correctly achieve the overriding objective – safety optimization. A reduction in the mean operational risk to a level of 25.62% was recorded relative to the shortest paths.

The next stage of the research involved conducting a comparative analysis of the arrival times of the ground emergency medical team (with a correction factor of k=0.7675) and the unmanned aerial vehicle. In order to quantify the time savings, two efficiency indicators were introduced: the absolute time savings (ΔT) and the relative time savings (δ).

The data presented in Table 8 indicate a clear advantage of UAV transport over road transport in terms of mission execution time. While the ambulance is forced to adapt its route to the geometry of the street network – resulting in high fluctuations in mean speed (ranging from approx. 32 to 50 km/h) – the LCP corridors provide a shorter, direct distance. As a result, the relative time savings δ range from 22% to 40% in favor of the UAV, and for the B-C relation, the drone reduced transport time by over 4.5 minutes (a 40% savings). However, it should be noted that UAV technology serves a complementary function in this system; due to design constraints and payload capacity limits, aerial transport does not replace the full functionality of an ambulance (associated with patient transport).

The data presented in Table 9 demonstrate an advanced analysis of the spatial structure of the BTS network (LTE800 standard) and the radio handover dynamics within a 1000 m buffer of the analyzed flight route centerlines, conducted using the ANN method and Voronoi polygons. An analysis of the spatial distribution index nn_{index} – which represents the ratio of the observed mean distance between stations (O_m) to the expected distance in a random distribution (E_m) – clearly demonstrates that the LCP algorithm modifies the spatial characteristics of the flight corridor. A key operational parameter is the number of UAV handovers between stations h_{UAV}, determined based on the number of intersections between a given trajectory and the boundaries of the Voronoi polygons. Importantly, the number of handovers does not differ significantly between the LCP and SP variants – for all route combinations, the mean geometric distance between successive handovers is approximately 609 m. Assuming a constant flight speed (v_{UAV}=15 m/s), this implies that the mean UAV operation time within the coverage area of a single transmitter (the handover procedure interval) is 40.62 s (Figure 5).

An analysis of the structure of relative time spent within individual planning zones confirms the effectiveness of the LCP algorithm in bypassing areas with a high level of urban risk. In the SP variant, the dominant spatial component is the flight over the multi-family residential zone (SW), which accounts for 33.4% of the time spent for the A-C route and reaches a critical value of as much as 60.8% for the B-C relation. Implementing the decision criteria of the AHP method and determining the LCP allowed for a reduction in the time spent in the SW zone to below 9%. As a result of the flight trajectory modification, the optimized routes were redirected over areas of low socio-economic sensitivity. Consequently, a distinct increase in the time spent by the UAV over these areas was recorded for the SI, SN, and SO zones compared to the short path.

When comparing the proposed framework with alternative path-planning algorithms such as A*, RRT*, or multi-objective optimization

Table 8. Comparison of distance and travel time between an emergency vehicle and a UAV flight between locations A, B, and C for the LCP (Variant 1)

Transport type	Routes		A-B	A-C	B-C
	Symbol	Parameter [unit]			
Ambulance (with warning signals)	L_{amb}	Length [m]	6400	7600	6200
	$T_{amb} \cdot k$	Time • *cor. factor* [min]	9.21	9.21	11.51
	V_{amb}	Mean velocity [km/h]	41.69	49.51	32.31
UAV for LCP	L_{UAV}	Length [m]	5328	5566	5355
	T_{UAV}	Flight time [min]	6.92	7.18	6.95
	ΔT	Time difference [min]	2.29	2.03	4.56
	δ	Time savings for UAV	25%	22%	40%

Table 9. ANN analysis results and the number of BTS handovers for individual designated UAV flight routes

Parameter	Routes between medical locations for Variant 1					
	A-B		A-C		B-C	
	LCP	SP	LCP	SP	LCP	SP
O_m	344.73	389.20	470.35	506.30	335.10	359.09
E_m	359.82	377.12	476.33	498.49	361.87	316.79
nn_{index}	0.96	1.03	0.99	1.02	0.93	1.13
z_{score}	-0.47	0.33	-0.12	0.14	-0.72	1.35
n	34	29	23	21	26	28
h_{UAV}	8	7	8	8	10	12

methods, the choice of a deterministic Least-Cost Path approach over classical A* is driven by the need for a global, wall-to-wall cumulative cost surface rather than isolated point-to-point heuristic searches. While A* is deterministic, it typically operates as a targeted node-to-node graph search, whereas the adopted multi-criteria evaluation framework evaluates continuous spatial resistance across the entire urban matrix, facilitating comprehensive spatial analysis. In contrast, sampling-based algorithms like RRT* and metaheuristic multi-objective methods are inherently stochastic,

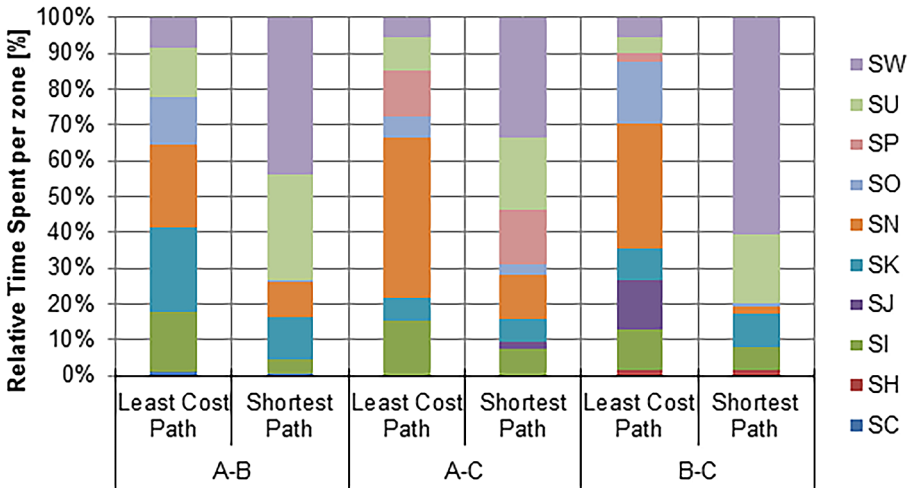


Figure 5. Graph showing the percentage structure of relative time spent by the UAV within individual planning zones for the least cost path (Variant 1) and shortest path. Designations: SW – multi-family residential zone, SU – service zone, SP – industrial zone, SO – open zone, SN – green and recreation zone, SK – transport zone, SJ – single-family residential zone, SI – infrastructure zone, SH – large-scale retail zone, SC – cemetery zone

introducing trajectory variability across independent runs. From a regulatory standpoint, municipal authorities require absolute predictability and spatial consistency. Because stochastic approaches yield fluctuating flight paths under identical constraints, such operational non-determinism is incompatible with real-world urban management. Consequently, the proposed deterministic framework bridges scientific rigor with practical utility, ensuring a fully reproducible and policy-compliant routing methodology.

CONCLUSIONS

This paper presents a universal, geoinformation methodology for planning safe UAV transport in medical logistics. This approach is based on multi-criteria evaluation of surface cost and can successfully mitigate operational risks in urban environments.

The main novelty consists in the direct integration of functional zones from emerging general municipal plans, combined with the application of dasymetric mapping for more accurate population density modeling. This allowed for an objective parametrization of ground risk and the determination of decision weights using the AHP method, while maintaining the aviation priority of protecting human life on the ground (with a cost weight of 50.28%).

Simulations performed for the city of Lublin revealed the superiority of the least-cost path (LCP) algorithm compared to conventional straight-line shortest paths. The overall operational risk to the population (R_{op}) was lowered to a mean value of 25.62% relative to the reference trajectories. This was achieved with an acceptable increase in path length of only 3.24–12.1%. Additionally, the flight duration over socially vulnerable high-density residential areas was reduced from an initial range of 33.4–60.8% to a level under 9%.

A time savings of 22% to 40% was achieved compared to a prioritized ground ambulance, reducing medical sample transport time by over 4.5 minutes in the extreme case. Furthermore, the model accounts for the stability of the command and control network based on BTS infrastructure.

Despite its demonstrated effectiveness as a strategic planning tool, the proposed methodology is subject to certain structural limitations that should be acknowledged. First, the current model relies on static demographic datasets and municipal planning zones, which do not capture diurnal human mobility patterns or real-time population shifts. Second, meteorological conditions - such as urban microclimates, localized wind fields, and turbulence - are treated as structural baselines rather than time-variant operational factors. Third, the Command and Control (C2) link assessment is based on the static geographic configuration of BTS infrastructure and Voronoi tessellation, omitting real-time cellular network traffic loads. Finally, the framework assumes static airspace designations, whereas mature UAM implementations will require adaptation to fixed or temporary constraints.

These identified limitations define clear pathways for the future expansion of the developed framework by incorporating critical dynamic factors. Subsequent research should focus on integrating temporal population distribution data to generate time-variant transport corridors optimized for peak traffic hours, working hours, and nighttime periods. Furthermore, incorporating real-time or forecasted weather conditions, dynamic communication quality metrics reflecting cellular network fluctuations, and real-time airspace restrictions will significantly enhance operational resilience.

Transitioning from static strategic planning to dynamic, multi-factor modeling will enable the evolution of the framework into an adaptive decision-support ecosystem, bridging rigorous regulatory compliance with the real-time operational demands of urban air mobility.

REFERENCES

1. Ayamga M., Akaba S., Nyaaba A. A. Multifaceted applicability of drones: A review. Technological Forecasting and Social Change. 2021; 167: 120677. https://doi.org/10.1016/j.techfore.2021.120677
2. Nisingizwe M.P., Ndishimye P., Swaibu K., et al. Effect of unmanned aerial vehicle (drone) delivery on blood product delivery time and wastage in Rwanda: a retrospective, cross-sectional study. Lancet Glob. Health 2022; 10(4): e564–e569. https://doi.org/10.1016/S2214-109X(22)00048-1
3. Thiels C.A., Aho J.M., Zietlow S.P., Jenkins D.H. Use of unmanned aerial vehicles for medical product transport. Air Med. J. 2015; 34(2): 104–108. https://doi.org/10.1016/j.amj.2014.10.011
4. Melo S., Silva F., Abbasi M., Ahani P., Macedo J. Public acceptance of the use of drones in city logistics: a citizen-centric perspective. Sustainability 2023; 15(3): 2621. https://doi.org/10.3390/su15032621

5. Smith A., Dickinson J.E., Marsden G., Cherrett T., Oakey A., Grote M. Public acceptance of the use of drones for logistics: The state of play and moving towards more informed debate. Technol. Soc. 2022; 68: 101883. https://doi.org/10.1016/j.techsoc.2022.101883
6. Scott J.E., Scott C.H. Drone Delivery Models for Healthcare. Proc. 50th Hawaii Int. Conf. System Sciences 2017: 3297–3304. http://hdl.handle.net/10125/41557
7. Singh T., Sinjana Y., Kapoor A.P. Aerial innovations in healthcare: A systematic review of drone-based logistics and regulatory barriers. J. Smart Future Transp. Res. 2026; 11: 101758. https://doi.org/10.1016/j.sftr.2026.101758
8. Mladenović M.N., Saif M.A., Honkavaara E., Kettunen P., Rönneberg M., Jussila A., Niemi L., Farstad M. A Collaborative GIS for Planning of Urban Drone Launch and Landing Site Locations. Int. Arch. Photogramm. Remote Sens. Spatial Inf. Sci. 2025; XL-VIII-2/W11-2025: 227–233. https://doi.org/10.5194/isprs-archives-XLVIII-2-W11-2025-227-2025
9. Nowakowski M., Berger G.S., Braun J., Mendes J., Bonzatto Junior L., Lima J. Advance reconnaissance of UGV path planning using unmanned aerial vehicle to carry our mission in unknown environment. Robot 2023: Sixth Iberian Robotics Conference 2024: 51–63. https://doi.org/10.1007/978-3-031-59167-9_5
10. Zhang Z., A review of unmanned aerial vehicle path planning techniques, Proceedings of the 2023 International Conference on Machine Learning and Automation, https://doi.org/10.54254/2755-2721/33/20230275
11. Act of 27 March 2003 on Spatial Planning and Land Development (Journal of Laws 2024, item 1415, as amended) [*pl. Ustawa z dnia 27 marca 2003 r. o planowaniu i zagospodarowaniu przestrzennym (Dz. U. z 2024 r. poz. 1415, z późn. zm.)]*.
12. Primatesta S., Guglieri G., Rizzo A. A risk-aware path planning strategy for UAVs in urban environments. Journal of Intelligent & Robotic Systems 2019; 95(2): 629–643. https://doi.org/10.1007/s10846-018-0924-3
13. Mennis J. Generating surface models of population using dasymetric mapping. The Professional Geographer 2003; 55(1): 31–42. https://doi.org/10.1111/0033-0124.10042
14. Clothier R. Safety Risk Management of Unmanned Aircraft Systems. Handbook of Unmanned Aerial Vehicles 2014: 1017–1043. https://doi.org/10.1007/978-90-481-9707-1_39
15. European Union Aviation Safety Agency (EASA). Easy Access Rules for Unmanned Aircraft Systems (Regulation (EU) 2019/947). Annex I - AMC1 to Article 11: Rules for conducting an operational risk assessment (SORA) 2019. https://www.easa.europa.eu/
16. Roca-Riu M., Menendez M. Logistic deliveries with Drones. State of the art of practice and research. Proc. 19th Swiss Transport Research Conference 2019. https://www.strc.ch/
17. Krawczyk Z., Vuppala R.K.S.S., Paul R., Kara K. Urban wind field effects on the flight dynamics of fixed-wing drones. Drones 2025; 9(5): 362. https://doi.org/10.3390/drones9050362
18. Adkins K., Wambolt P., Sescu A., Swinford C., Macchiarella N.D. Observational practices for urban microclimates using meteorologically instrumented unmanned aircraft systems. Atmosphere 2020; 11(9): 1008. https://doi.org/10.3390/atmos11091008
19. Chan Y.Y., Ng K.M.H., Lee C.K.M., Hsu L.T., Keung K.L. Wind dynamic and energy-efficiency path planning for unmanned aerial vehicles in the lower-level airspace and urban air mobility context. Sustain. Energy Technol. Assess. 2023; 57: 103202. https://doi.org/10.1016/j.seta.2023.103202
20. Amorim R., Nguyen H., Mogensen P., Kovács I.Z., Wigard J., Sørensen T.B. Radio channel modeling for UAV communication over cellular networks. IEEE Wireless Commun. Lett. 2017; 6(4): 514–517. https://doi.org/10.1109/LWC.2017.2712152
21. Lin X., Yajnanarayana V., Muruganathan S.D., Gao S., Asplund H., Maattanen H.L. The sky is not the limit: LTE for unmanned aerial vehicles. IEEE Commun. Mag. 2018; 56(4): 204–210. https://doi.org/10.1109/MCOM.2018.1700643
22. Shapira M., Cohen B., Friemann S., Tal Y., Teper Z., Dudkiewicz M., Portuguese S., Na'amnih W., Dahan Shriki D. The impact of clinical sample transportation by unmanned aerial systems on the results of laboratory tests. Drones 2025; 9(3): 179. https://doi.org/10.3390/drones9030179
23. Callewaert N., Pareyn I., Acke T., Desplinter B., Van de Pitte K., Van Vooren J., De Meyer M., Seeldraeyers E., Peeters F., De Meyer S.F., Vanhoorelbeke K., Tersteeg C. Limited impact of drone transport of blood on platelet activation. Drones 2024; 8(12): 752. https://doi.org/10.3390/drones8120752
24. Jansson P.S., Richards J.B., Frakes M.A., Cohen J.E., Wilcox S.R. the effect of lights and sirens on critical care transport time. J. Emerg. Med. 2020; 59(4): 553–560. https://doi.org/10.1016/j.jemermed.2020.06.066
25. Joint Authorities for Rulemaking on Unmanned Systems (JARUS). JARUS Guidelines on SORA. Annex F: Theoretical Basis for Ground Risk Classification and Mitigation, Edition 2.5 (JAR-DEL-SRM-SORA-F-2.5, JAR doc 29) 2024. http://jarus-rpas.org
26. Head Office of Geodesy and Cartography, 2026. Topographic Object Database (BDOT10K). [data set] Available at: https://www.geoportal.gov.pl [Accessed June 2026].